Acta Scientiarum
http://periodicos.uem.br/ojs
ISSN on-line: 1807-8664
https://doi.org/10.4025/actascitechnol.v48i1.73241

Modelling the dispersion of pollutants in the water supply of a metropolis in the Amazon

Romulo Correa Lima[1], Claudio José Cavalcante Blanco[2*], André Luiz Amarante Mesquita[3] and Yves Secretan[4]

[1]Faculdade de Ciências Exatas e Tecnologia, Universidade Federal do Pará, Abaetetuba, Pará, Brasil. [2]Laboratório de Engenharia Hídrica e Mudanças Climáticas, Universidade Federal do Pará, Rua Augusto Corrêa 1, Guamá, 66075-110, Belém, Pará, Brasil. [3]Programa de Pós-Graduação em Engenharia de Recursos Naturais da Amazônia, Universidade Federal do Pará, Belém, Pará, Brasil. [4]Institut National de la Recherche Scientifique – Eau, Terre et Environnement, Université du Québec, Québec, Canadá. *Author for correspondence. E-mail: blancocjc@outlook.com

ABSTRACT. Belém, the capital of the state of Pará and the host city of COP30 (30th United Nations Climate Change Conference), located in the Brazilian Amazon, faces a risk to its potable water source due to pollution. Thus, the study aims to model the dispersion of pollutants, in this case, phosphorus, within the Utinga source, which is formed by the artificial lakes Água Preta and Bolonha. The Saint-Venant equations were solved via a hydrodynamic model formulated with the finite element method. Pollutant dispersion simulation followed the SUPG/θ numerical method for spatial and temporal discretization, respectively, of the advection-diffusion-reaction equation in two dimensions. The results indicate that, due to the low flow dynamics of the lakes, the highest phosphorus concentration is found near the entry of Lake Água Preta. This is a result of the waters from the Guamá River, which receive a significant portion of the city of Belém's sewage, only 2.38% of which is treated. A good legacy of COP30 would be a sewage collection and treatment system for Belém, which would minimize the pollution of the waters of the Guamá River and, consequently, the waters of the Utinga source benefiting the region's population.

Keywords: COP30, lake pollution, phosphorus, numerical simulation, finite elements method.

Received on August 02, 2024.
Accepted on June 25, 2025.

Introduction

Hydrodynamic and pollutant transport simulations are important tools for studying and managing bodies of water. This computational approach combines hydrodynamic models and pollutant transport models to understand and predict the flow and spread of pollutants in these aquatic systems. Understanding how water flows and how pollutants are transported is necessary for assessing environmental risks, identifying contamination areas, and developing effective strategies for mitigating environmental disasters. Numerous studies have been dedicated to this topic. Streeter-Phelp's work in 1925 was one of the earliest developments which analysed the self-purification process of a polluted watercourse by considering atmospheric reaeration processes (McCartin & Forrester Jr., 2002). Mathematical models have since become more complex, and with increased computational capabilities, it has become possible to develop more realistic models. For example, Elshemy et al. (2016) developed a hydrodynamic and water quality model for Lake Manzala, Egypt, using the MIKE21 modelling system. The model results showed good agreement with the observed water depth, water temperature, and salinity records. The model was intended to be used to investigate the impacts of future climatic changes on the hydrodynamic and water quality characteristics of the lake.

Yi et al. (2017) developed a hydrodynamic model associated with a water quality model to understand the flow of possible pollutants in a water transfer project. The project studied the transfer of water from the Danjiangkou Reservoir to Lake Tuancheng and was constructed mainly to supply drinking water for cities in North China, including the capital city of Beijing. Roohi et al. (2020) numerically evaluated the general flow hydraulics and estimates of the Mehrian River floodplain in Iran. The results were compared to the results of the Att-Kin and Muskingum models. The authors noted that the MIKE 11 dynamic wave model produced the best results. More recently, Tarabih et al. (2023) presented a Python-based model combining three modules: one for simulating hydrology, another for simulating phosphorus dynamics in

the water column, and an optimization tool for designing optimal discharges. By using this code in a study of Lake Okeechobee (Florida, USA), they concluded that the phosphorus load could vary from 12% to 33% using optimization operations.

Coming to the present study, the Utinga source, which is composed of the artificial lakes Água Preta and Bolonha, serves as a reservoir for the city of Belém and its metropolitan region. Several studies have been conducted on the analysis of dynamics and/or pollutant transport in these lakes. Initially, the flows of the lakes were simulated separately. Holanda et al. (2011) presented hydrodynamic modelling of Lake Água Preta and concluded that velocities within the lake ranged from 0.00 to 0.33 ms^{-1}, with the highest velocity being reached at the entrance of the interconnection channel with Lake Bolonha. Lima et al. (2013) presented hydrodynamic modelling of Lake Bolonha and concluded that velocities within the lake ranged from 0.00 to 0.18 ms^{-1}, with the highest velocity being reached at the water intake of the Bolonha Water Treatment Plant (WTP).

Regarding pollutant dispersion, Lima et al. (2015) used the θ/SUPG method to analyse phosphorus behaviour in Lake Água Preta. The phosphorus sources analysed were water pumped from the Guamá River received by the lake and point sources due to disorderly occupation occurring along the lake shores. The authors concluded that phosphorus concentration rates increased with increased rainfall in the region, as they contributed to transporting phosphorus from point sources to lake shores. Santos et al. (2015) collected and analysed the concentrations of metals and phosphorus present in the sediment samples from Lake Água Preta. The data indicated a reservoir with nonuniform sediments and a relatively high fraction of granular mud. Inorganic phosphorus was predominantly found. On the other hand, the nickel, copper, lead, and zinc concentrations were below the probable effect level (PEL). However, nickel and lead concentrations were above the suggested threshold effect level (TEL), indicating that humans influence lake contamination. Araújo et al. (2021) analysed the flows of two lakes plus the connecting channel, i.e., the Utinga source flow was simulated integrally. The authors found velocities ranging from 0.00 to 0.24 ms^{-1}. In this case, the maximum velocity (0.24 ms^{-1}) is lower than the velocity when considering only the simulation of Água Preta Lake flow, which was equal to 0.33 ms^{-1} (Holanda et al., 2011). This difference in results can be explained by the complete simulation of the Utinga source, unlike the articles of Holanda et al. (2011) and Lima et al. (2013), who simulated the flows of Bolonha and Água Preta lakes separately.

Our current objective is to present a 2D simulation of the flow and dispersion of phosphorus in the Utinga source, from the entry point of water pumped from the Guamá River to the water intakes at two treatment stations, namely, the Bolonha Lake Water Treatment Plant (WTP1) and the São Braz Water Treatment Plant (WTP2). In this case, the hydrodynamic model developed by Araújo et al. (2021) serves as the basis for the phosphorus dispersion simulations, which were implemented using the model developed by Lima et al. (2015), as previously cited. Belém was chosen by the United Nations (UN) to host COP30 (30th UN Conference on Climate Change). Therefore, a project to increase the volume of treated sewage in the city, currently not exceeding 2.38% (Instituto Trata Brasil, 2024), would be a significant legacy of COP30 for the people of Belém do Pará, contributing to the reduction of pollutants carried by the waters of the Guamá River and treated in the Utinga source. In this context, the work aligns with UN Sustainable Development Goal 6, which focuses on clean water and sanitation (Organização das Nações Unidas [ONU], 2015). The results of this study can provide valuable scientific support for decision-making during COP30 discussions related to urban planning, sanitation infrastructure, and environmental protection strategies in the Amazon region.

Material and methods

Study Area

In the Amazon region of Brazil is the state of Pará, whose capital, Belém, and its metropolitan area obtain their potable water supplies from the waters taken from the Guamá River and stored in the Água Preta and Bolonha Lakes. Figure 1 depicts an artificial canal interconnecting these lakes. Lake volumes are maintained through water pumped from the Guamá River to Água Preta Lake. The system formed by the lakes is referred to as the Utinga source, with its waters treated at two stations. WTP1 is located on the shores of Lake Bolonha (Figure 1). However, WTP2 is in the São Braz neighbourhood, approximately 7.5 km away from Lake Bolonha. The water reaches WTP2 via a pipeline, indicated in Figure 1 as the output.

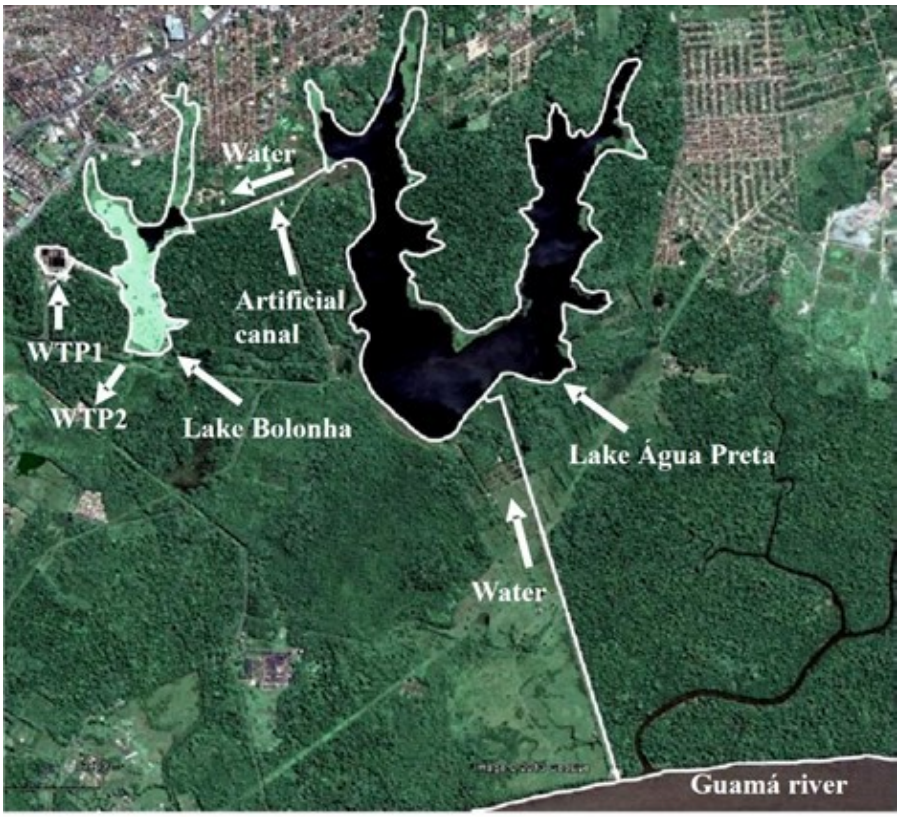

Figure 1. Water circuit in the Utinga system from collection in the Guamá River to outlets for treatment plants.
Adapted from Google Earth (2024) retrieved from https://earth.google.com/.

Hydrodynamic model

The initial step for simulating pollutant transport in an aquatic environment involves generating hydrodynamic models. Thus, the Saint-Venant model or shallow water model was utilized. The main conditions to be fulfilled for using this model (Heniche et al., 2000) are given below:

- the water column is mixed in the vertical direction, and the depth is small compared to the width and length of the water volume;

- waves have low amplitudes and long periods (tide waves). The vertical acceleration component is negligible, allowing for a hydrostatic pressure approximation.

(Equation 1) to (Equation 3) are conservative forms of the Saint-Venant equations. The first is the continuity equation, whereas the other two are the momentum conservation equations for the fluid in the x and y directions, respectively.

$$\frac{\partial h}{\partial t} + \frac{\partial q_x}{\partial x} + \frac{\partial q_y}{\partial y} = 0 \quad (1)$$

$$\frac{\partial q_x}{\partial t} + \frac{\partial q_x \frac{q_x}{H}}{\partial x} + \frac{\partial q_x \frac{q_y}{H}}{\partial y} = \sum F_x \quad (2)$$

$$\frac{\partial q_y}{\partial t} + \frac{\partial q_y \frac{q_x}{H}}{\partial x} + \frac{\partial q_y \frac{q_y}{H}}{\partial y} = \sum F_x \quad (3)$$

where q_x and q_y are the flow rates in Cartesian coordinates x and y, respectively; t is time; h is the water level; H is the depth of the water column; and F_x and F_y are the volume forces in the x and y directions, respectively.

F_x and F_y are given by (Equation 4) and (Equation 5).

$$\sum F_x = -gH\frac{\partial h}{\partial x} - \frac{n^2 g|\vec{q}|q_x}{H^{\frac{7}{3}}} + \frac{1}{\rho}\left(\frac{\partial(H\tau_{xx})}{\partial x}\right) + \frac{1}{\rho}\left(\frac{\partial(H\tau_{xy})}{\partial y}\right) + F_{cx} + F_{wx} \quad (4)$$

$$\sum F_y = -gH\frac{\partial h}{\partial y} - \frac{n^2 g|\vec{q}|q_y}{H^{\frac{7}{3}}} + \frac{1}{\rho}\left(\frac{\partial(H\tau_{yx})}{\partial x}\right) + \frac{1}{\rho}\left(\frac{\partial(H\tau_{yy})}{\partial y}\right) + F_{cy} + F_{wy} \quad (5)$$

where g is the acceleration of gravity; n is the Manning coefficient; $|\vec{q}|$ is the modulus of the specific flow rate; ρ is the water density; and τ_{ij} is the Reynolds stress tensor (Equation 6).

$$\tau_{ij} = \nu\left(\frac{\partial\overline{U_i}}{\partial x_j} + \frac{\partial\overline{U_j}}{\partial x_i}\right) \quad (6)$$

F_{cx} and F_{cy} are the Coriolis forces in the x and y directions, respectively, and F_{wx} and F_{wy} are the wind forces in the x and y directions, respectively. The influence of wind was not considered, and the Coriolis effect was ignored due to the position of the domain close to the equator. The turbulence model employed was the mixing length (L_m), or rather, the distance between the wall and a point in the flow from which the wall itself no longer affects turbulence. The model provides a balance between the creation and dissipation of energy. In this case, the turbulence viscosity is given by (Equation 7).

$$\upsilon_t = L_m^2\sqrt{2D_{ij}D_{ij}} \quad (7)$$

where ν_t is the turbulence viscosity and D_{ij} is the ij component of the deformation tensor, given by (Equation 8).

$$D_{ij} = \frac{1}{2}\left(\frac{\partial\overline{U_i}}{\partial x_j} + \frac{\partial\overline{U_j}}{\partial x_i}\right) \quad (8)$$

where $\overline{U_i}$ is the mean velocity in the i direction.

H2D2 and finite elements method

The development of hydrodynamic modelling primarily requires substrate and topography data, which are employed to assemble the terrain elevation model (TEM), whereas substrate composition data are used for setting the Manning coefficient. The TEM plus roughness model and boundary conditions provided the data for the Saint-Venant equation solution, allowing for the simulation of velocities and depths of lakes Água Preta, Bolonha and the interconnection canal (Figure 1). H2D2 (Secretan, 2023) academic software, developed at INRS-ETE, a research centre of Université du Québec, Canada (Heniche et al., 2000), was used in the current analysis. Studies by Holanda et al. (2011), Lima et al. (2013), Holanda et al. (2017) and Araújo et al. (2021) have corroborated the efficiency of the model and its applicability.

H2D2 is a combination of a geographic information system (GIS) and a powerful pre- and postprocessor finite element method, allowing the establishment of TEMs with information concerning topography, riverbed substrate, wind, ice, and aquatic plants. H2D2 also enables the division of the analysed region into partitions. The TEM datasets are associated with the partitions. An automatic procedure of data treatment at the interfaces of the partitions is used for the mesh generation of finite elements, which will be used to solve the 2-D Saint-Venant model with a drying/wetting capability to follow shoreline evolution. The finite elements consist of six-node triangles of six nodes, called T6L (Figure 2). The variables h (water level), H (depth), zf (share fund) and n (Manning coefficient) are linearly interpolated because their gradients are less pronounced than those of the velocities U and V and specific flow rates q_x and q_y, which are interpolated quadratically by generally steeper gradients.

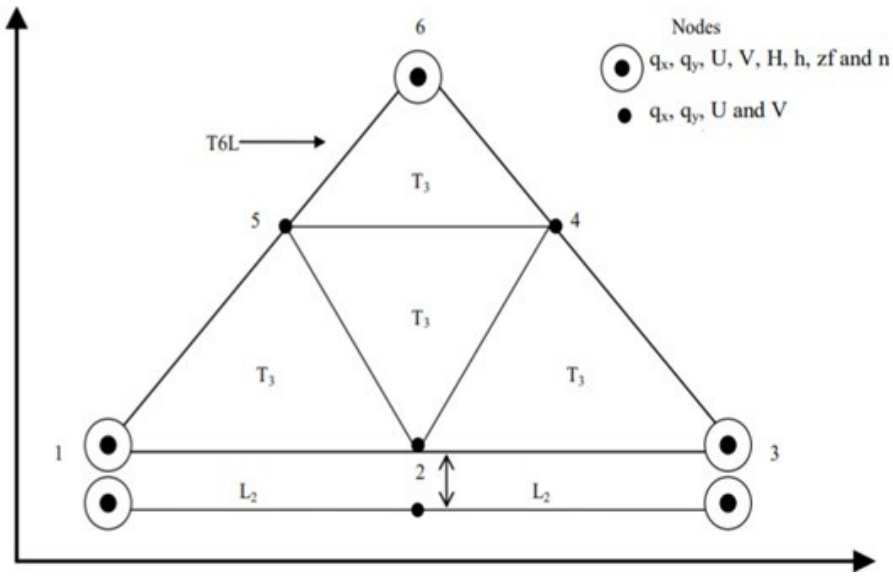

Figure 2. Triangulation used by H2D2.

Pollutant dispersion model

Let Ω be a bounded domain in R^2, with boundary Γ. Let $C(z,t)$ be a scalar quantity to be transported (e.g., mass concentration). The problem consists of finding C that satisfies the transport equation (Equation 9).

$$\frac{\partial C}{\partial t} + u.\nabla C - \nabla.(D\nabla C) + r = 0 \; on \; (\Omega, t) \tag{9}$$

where t is the temporal variable; $z = (x,y) \in R^2$ is the spatial vector; u is the velocity field; D is the diffusivity coefficient; r refers to processes that produce or consume the species of interest through chemical, physical, or biological transformations within the body of water, referred to as homogeneous reactions, whereas nonhomogeneous reactions represent sources or sinks that occur only at fluid boundaries. In this study, first-order reaction kinetics were adopted, which can be expressed as (Equation 10) (Lima et al., 2015).

$$\frac{\partial C}{\partial t} + u.\nabla C - \nabla.(D\nabla C) + kC = 0 \tag{10}$$

where *k* represents the reaction coefficient. This equation is subject to the initial condition within the domain as specified in (Equation 11).

$$C(z,0) = C_0(z) \; on \; (\Omega, t = 0) \tag{11}$$

and the boundary condition (Equation 12),

$$\partial C/\partial z|_n = 0 \tag{12}$$

on the solid boundaries (Equation 13), where *n* is the normal vector to this boundary, and

$$C = g(z,t) \; on \; z = \Gamma \tag{13}$$

at the domain inlet, where *g* is a function representing the intake of mass concentration from outside the domain. For the conditions at the exit boundaries of the domain (Equation 14), it is assumed that the concentrations in the inner and outer vicinity of these boundaries are equal (Massabó et al., 2011), i.e.,

$$\partial C/\partial z|_{out} = 0 \tag{14}$$

Time discretization – θ method

Temporal discretization by the θ method involves a weighted average of the equation terms at times *n* and *n+1*. Thus, (Equation 10) is written in the following form (Lima et al., 2014):

$$\frac{C^{n+1} - C^n}{\Delta t} + \theta(u.\nabla C)^{n+1} + (1-\theta)(u.\nabla C)^n - \theta[\nabla.(D\nabla C)]^{n+1} -$$
$$(1-\theta)[\nabla.(D\nabla C)]^n + \theta(kC)^{n+1} + (1-\theta)(kC)^n = 0 \tag{15}$$

where C^n is the approximation of $C(t_n)$, with $t_n = t_0 + n\Delta t$, where t_0 is the initial time, $\Delta t = t_n - t_{n-1}$, and θ is the parameter that determines which finite difference method will be used. Depending on the value of $\theta \in [0,1]$, various methods can be obtained, with the most common being explicit (θ = 0), Crank-Nicolson (θ = 1/2), and implicit (θ = 1). For values of $\theta \geqslant 0.5$, the methods will be unconditionally stable. After algebraic manipulation, (Equation 15) can be rewritten as

$$\frac{C^{n+1} - C^n}{\Delta t} + \theta(u.\nabla C)^{n+1} - \theta(u.\nabla C)^n - \theta[\nabla.(D\nabla C)]^{n+1} + \theta[\nabla.(D\nabla C)]^n + \theta(kC)^{n+1} - \theta(kC)^n =$$
$$-(u.\nabla C)^n + [\nabla.(D\nabla C)]^n - (kC)^n \tag{16}$$

By setting $\Delta C = C^{n+1} - C^n$, one can write (Equation 16) in the following form (Equation 17):

$$\frac{\Delta C}{\Delta t} + \theta[u.\nabla - \nabla.(D\nabla) + k]\Delta C = -[u.\nabla - \nabla.(D\nabla) + k]C^n \tag{17}$$

Finite element discretization - basic formulation

At this point, one must construct a finite element mesh Ω_h generated by the union of the finite elements Ω_e to represent an approach of the domain Ω (Equation18), such that

$$\Omega \cong \Omega_h = e = 1nel\Omega_e \wedge \Omega_e \cap \Omega_f = \emptyset, \forall e \neq f \tag{18}$$

where *nel* represents the number of finite elements. Each subdomain Ω_e has a smooth contour Γ_e.

Spatial discretization by finite elements relies on a discretized representation of a weak integral form of (Equation 17). The formulation and subsequent discretization of this integral requires the definition of some function spaces and associated norms. In the Galerkin formulation sense, one must approach the infinite-dimensional spaces for appropriated finite subsets of that collection, which is denoted by V^h and S_t^h). The basic idea is to represent approximated solutions $w_h \in V^h$ and test functions $C_h \in S^h$ in each Ω_e so that

$V^h = \{w \in H^1(\Omega) | w|_{\Omega_e} \in P_p(\Omega_e) \forall e \wedge w|_{\Gamma_D} = 0\}$,

$S_t^h = \{C | C(.,t) \in H^1(\Omega), C(.,t)|_{\Omega_e} \in P_p(\Omega_e) \forall e \wedge C|_{\Gamma_D} = C_D\}$

where $H^1(\Omega)$ is the Sobolev space with a square integrable derivative and P_p is the polynomial interpolation space of order p. At this point, it is necessary to apply the variational formulation to (Equation 17), yielding the following integral formulation:

$$\int_\Omega w \frac{\Delta C}{\Delta t} d\Omega + \int_\Omega w\theta[u.\nabla - \nabla.(D\nabla) + k]\Delta C d\Omega = -\int_\Omega w[u.\nabla - \nabla.(D\nabla) + k]C^n d\Omega \quad (19)$$

The approximated function C_h in each element can be written as (Equation 20):

$$C \approx C_h = \sum_{i=1}^{r} N_i C_i = NC \quad (20)$$

where r is the number of nodes in each Ω_e, N is the basis function vector and C is the vector containing the nodal values of variable C. Therefore, one can write (Equation 19), after substitution of (Equation 20) and some algebraic manipulations and application of the boundary conditions, as (Equation 21):

$$\frac{\Delta C}{\Delta t}\int_\Omega wNd\Omega + \theta\left\{\int_\Omega w[u.\nabla N - \nabla.(D\nabla N) + kN]d\Omega\right\}\Delta C = -\left\{\int_\Omega w[u.\nabla N - \nabla.(D\nabla N) + kN]d\Omega\right\}C^n + \int_{\Gamma_N} w[\theta b^{n+1} + (1-\theta)b^n]d\Gamma_N \quad (21)$$

SUPG method

This method consists of the summation of a perturbation term $P(N)$, the weighting function of the Galerkin method, in a consistent way, as shown in (Equation 22).

$$w = N + \tau P(N) \quad (22)$$

where τ is the stabilization parameter. Many studies have been devoted to determine this parameter. This study follows the works of Tezduyar (1992), who reported that for the transient advection–diffusion equation, which is semidiscretized in time by the θ-method, the τ parameter can be given as (Equation 23).

$$\tau = \left(\frac{1}{\theta\Delta t} + \frac{2|u|}{h} + \frac{4D}{h^2} + k\right)^{-1} \quad (23)$$

Among the resulting methods of (Equation 22), one has the SUPG method through the definition of $P(N)$ as (Equation 24).

$$P(N) = \frac{h}{2}\frac{u}{|u|}\nabla N = \frac{\Delta t}{2}u\nabla N \quad (24)$$

Substituting (Equations 22) and (Equations 24) in (Equations 21), one obtains, after algebraic manipulation, (Equation 25),

$$\frac{\Delta C}{\Delta t}\left[\int_\Omega NNd\Omega + \int_\Omega \alpha u\nabla NNd\Omega\right] + \theta\left\{\int_\Omega Nu.\nabla Nd\Omega + \int_\Omega \alpha(u.\nabla N)(u.\nabla N)d\Omega + \int_\Omega D\nabla N.\nabla Nd\Omega + \int_\Omega D\alpha(u.\nabla^2 N).\nabla Nd\Omega + \int_\Omega kNNd\Omega + \int_\Omega k\alpha(u.\nabla N).\nabla Nd\Omega\right\}\Delta C = -\left\{\int_\Omega Nu.\nabla Nd\Omega + \int_\Omega \alpha(u.\nabla N)(u.\nabla N)d\Omega + \int_\Omega D\nabla N.\nabla Nd\Omega + \int_\Omega D\alpha(u.\nabla^2 N).\nabla Nd\Omega + \int_\Omega kNNd\Omega + \int_\Omega k\alpha(u.\nabla N).\nabla Nd\Omega\right\}C^n + \int_{\Gamma_N}(N + \alpha u.\nabla N)[\theta b^{n+1} + (1-\theta)b^n]d\Gamma_N. \quad (25)$$

where $\alpha = \tau\Delta t/2$.

Writing $\Delta C = C^{n+1} - C^n$ and each integral in matrix form as

$$M = \int_\Omega NNd\Omega,$$

$$A = \int_\Omega u\nabla NNd\Omega,$$

$$K = \int_{\Omega} D\nabla N.\nabla N d\Omega,$$

$$K_1 = \int_{\Omega} (u.\nabla N)(u.\nabla N) d\Omega,$$

$$K_2 = \int_{\Omega} D(u.\nabla^2 N).\nabla N d\Omega,$$

$$F = \int_{\Gamma_N} (N + \alpha u.\nabla N)[\theta b^{n+1} + (1-\theta) b^n] d\Gamma_N$$

and after algebraic manipulation, (Equation 25) can be rewritten as (Equation 26).

$$[M + \alpha A + \theta \Delta t M] C^{n+1} = [M + \alpha A + (\theta - 1)\Delta t M] C^n + \Delta t F \quad (26)$$

where

$$M = A + K + \alpha(K_1 + K_2) + k(M + \alpha A)$$

This linear system is derived using the SUPG/θ method for a transient advection-diffusion-reaction equation. All the global matrices in this equation remain constant throughout the temporal evaluation, requiring calculation only once. However, (Equation 26) represents a large, sparse linear system. The optimal approach for solving this problem involves applying an iterative method solver designed for such systems. Among the various methods available, the most employed and extensively studied is the generalized minimal residual method (GMRES), which approximates the solution by minimizing the residual vector within a Krylov subspace (Saad & Schultz, 1986).

Boundary conditions

Another underlying element for the formulation of the hydrodynamic model includes the appropriate boundary conditions (free surface, bottom and closed, moving or open boundaries), which comprise entrance rates or output flows or properties, in accordance with the boundary typology. The conditions in the current study are solid boundaries, impermeability conditions, liquid boundaries, water levels and outflows. Figure 3 shows the boundary conditions for maximum flow in lakes Bolonha and Água Preta. A: Water intake through the Guamá River, flow = 6.0 $m^3 s^{-1}$ and water level = 8.9 m; B: Water outlet of the Bolonha Lake, flow = 1.8 $m^3 s^{-1}$ and water level = 7.0 m; C: Water outlet of the Bolonha Lake, flow = 4.2 $m^3 s^{-1}$ and water level = 7.0 m (Lima et al., 2013; Holanda et al., 2011). The boundary conditions for the phosphorus transport simulation are given by Eqs. 12 to 14.

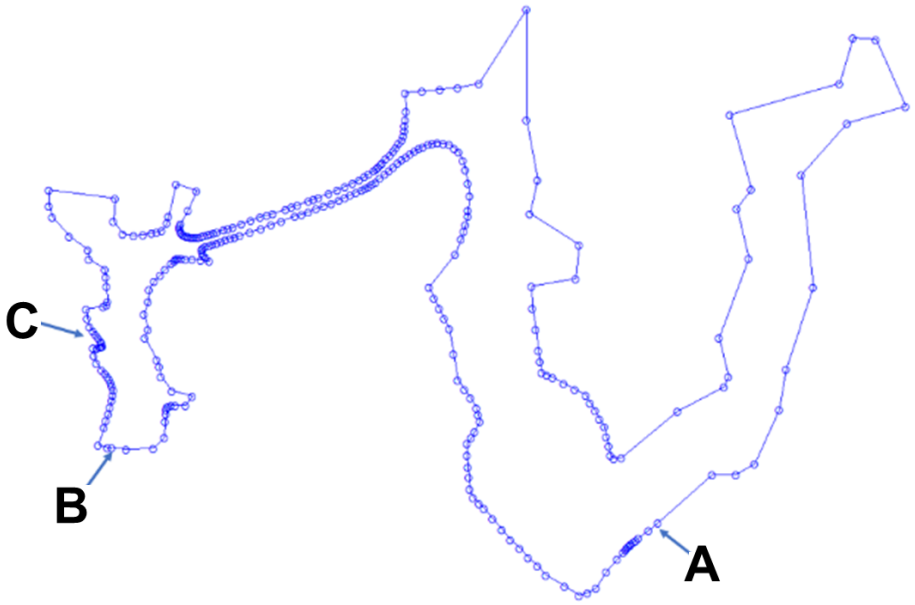

Figure 3. Boundary conditions applied to the domain of simulation.

Calibration model

The model calibration was based on the Manning friction coefficient with values of 0.019 s $m^{-1/3}$ for the Bolonha and Água Preta lakes, and equal to 0.020 s $m^{-1/3}$ for the interconnecting channel of the lakes (Araújo et al., 2021). These values were applied to a mesh with 46,094 elements and 94,705 nodes and a mesh refining with the larger edge of the triangles for the finite elements equal to 7 m (Figure 4). Thus, the relative percentage error between the simulated flows and those of the boundary conditions was 5.9%.

Results and discussion

Hydrodynamic mesh

Figure 4 shows the hydrodynamic mesh with triangular finite elements used in the simulations for the Utinga water source. The mesh stores all the input variables required for the resolution of the Saint-Venant equations and the resulting variables for the simulation of the two-dimensional flow (U, V and H). For the model considered herein, the input variables are the following: the x, y and z, interpolated via the TEM and transferred to the hydrodynamic mesh; the Manning friction coefficient calculated value; and the boundary conditions defined previously.

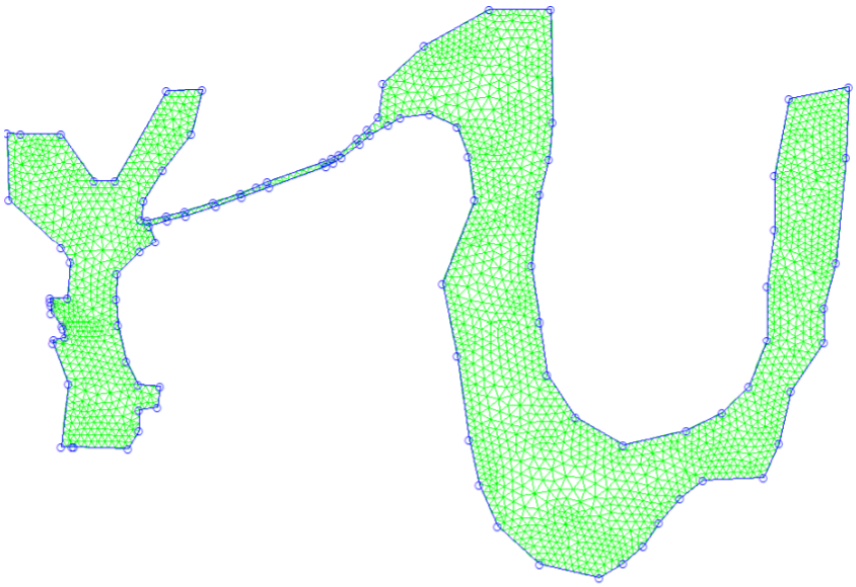

Figure 4. Hydrodynamic mesh of the lakes Bolonha and Água Preta and the interconnection canal.
Araújo et al. (2021).

Terrain elevation model

Figure 5 shows the TEM interpolated and projected on the hydrodynamic mesh. Thus, the topography represented by the isosurfaces indicates the levels within the lakes and the canal. It reveals, as expected, that the region further to the north of the lakes has greater elevations since the springs to the creeks making up the lakes are in that region. The topographical elevations vary from 1.01 m to 14.54 m. The minimum elevation is in the central region of Lake Bolonha. In general, the interpolated TEM adequately represents the topography of the Utinga source, which is very important for the success of hydrodynamic simulations. Moreover, the topography rates observed for the lakes corroborate the results of Holanda et al. (2011) for Lake Água Preta and Lima et al. (2013) for Lake Bolonha. This is the first time that the topography of an interconnection canal has been numerically analysed.

Velocities

An analysis of Figure 6 reveals that the system maintains its reservoir characteristics, with velocities close to 0 (zero). The flow is accelerated only at its liquid boundaries: the water inlet in Lake Água Preta, the water outlet of Lake Bolonha and the interconnection canal. The flow velocity close to the water inlet and outlet of Lake Água Preta is equal to 0.06 ms^{-1}, which is in line with that determined by Holanda et al. 2011. Furthermore, the flow velocity near the water inlet of Lake Bolonha is approximately 0.10 ms^{-1}. The flow

velocities near the central water outlet and south of Lake Bolonha are 0.24 ms^{-1} and 0.20 ms^{-1}, respectively. These rates are slightly higher than those determined by Lima et al. (2013), who reported rates of 0.18 ms^{-1} and 0.14 ms^{-1} for the same locations, respectively. These differences in results may be explained by the complete simulation of the Utinga source, which is different from that of other studies that simulated the flows of Lakes Bolonha and Água Preta separately. The flow simulation in the interconnection canal with higher velocities varied between 0.119 ms^{-1} and 0.238 ms^{-1}. This is the first time that the flow in an interconnection canal has been analysed.

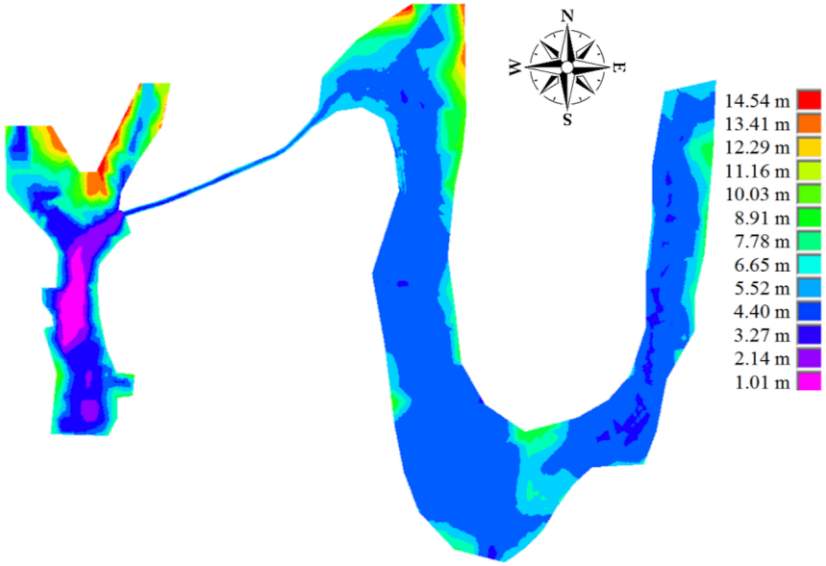

Figure 5. TEM projected and interpolated on the hydrodynamic mesh of the Utinga source in isosurfaces.
Araújo et al. (2021).

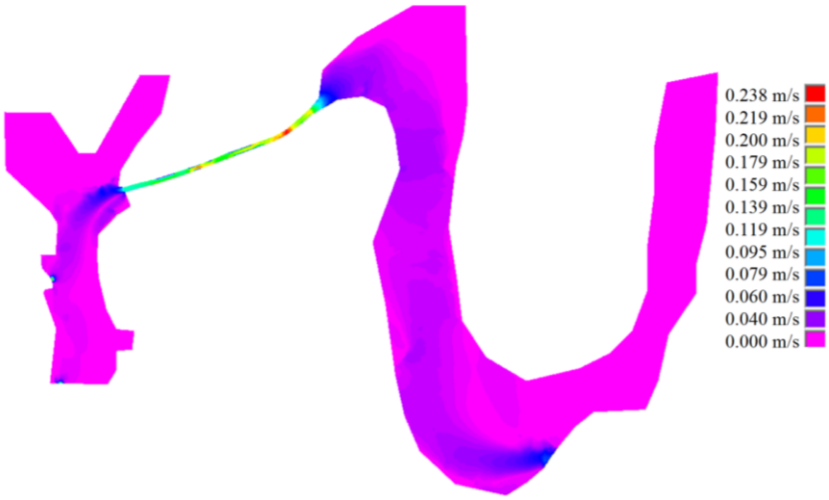

Figure 6. Velocities of the isosurfaces of the Utinga water source.
Araújo et al. (2021).

Figure 7 shows the composition of the vector and scalar velocity field, highlighting that the highest velocities are in the connecting channel due to the reduced cross-sectional area for flow, while the lowest velocities are in Lake Água Preta, reflecting the reservoir-like characteristics of this lake.

Phosphorus transport

The behaviour of phosphorus dispersion, as well as the time required from its entry into Lake Água Preta until it reaches the intakes of the Bolonha and São Braz Water Treatment Plants in Lake Bolonha, was analysed. In this case, a constant input of the pollutant with diffusion coefficients $D_x = D_y = 9 \times 10^{-2}\, m^2/s$ and reaction coefficient $k = 3 \times 10^{-6}\, 1/s$ was considered. Furthermore, the velocity field presented in the previous section was assumed to be unchanged, resulting in the temporal sequence shown in Figure 8.

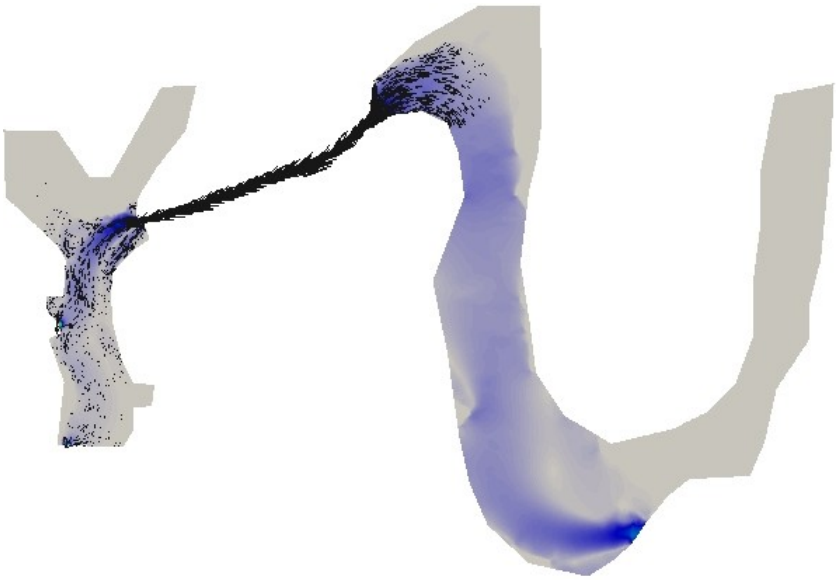

Figure 7. Vector and scalar velocity field in the Utinga source.

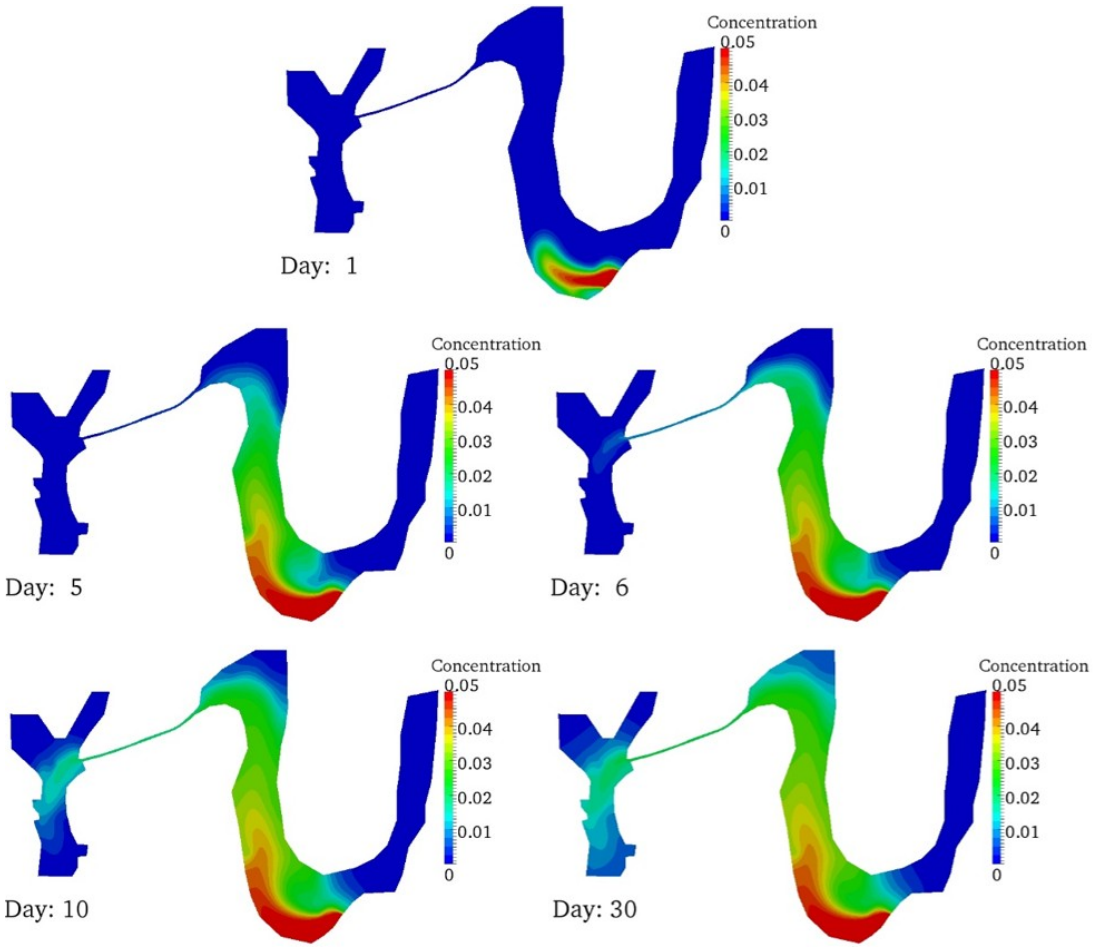

Figure 8. Evolution of phosphorus dispersion from its entry into Lake Água Preta until it reaches the outlets of Lake Bolonha and its spreading therein.

Analysing this figure, it can be observed that due to the low velocities throughout the lakes, after the first day when the pollutant enters Lake Água Preta, its concentration accumulates in the region near the conduit that transports water from the Guamá River. The contaminant begins to reach the lake's outlet in the interconnection channel from the fifth day, with concentrations below 0.02 mg L^{-1}, as it already occupies the entire channel with the highest hydraulic velocity within the lake. On the sixth day, the pollutant starts to cross the connecting channel, reaching Lake Bolonha with concentration values below 0.01 mg L^{-1}. By the

tenth day, the pollutant reaches an average concentration of 0.01 mg L^{-1} at the entrance of the WTP1 treatment plant but has not yet reached WTP2, which is only reached around the twentieth day due to the extremely low velocities within Lake Bolonha. From that point onwards, the concentration values continuously increase in both lakes until stabilizing after the twenty-fifth day, with the contaminant concentration remaining at approximately 0.02 mg L^{-1} at WTP1 and 0.01 mg L^{-1} at the entrance of WTP2, while near the conduit region, it exceeded 0.05 mg L^{-1}. Thus, it can be estimated that the entry of a pollutant from the Guamá River may take approximately one week to reach the entrance of the first treatment plant and reaching the second plant in approximately twenty days. Its concentration reaches a maximum level in approximately 25 days throughout the Utinga source.

Conclusion

During the analysis of the computed velocities in the Utinga source, it was observed that most of the area maintains reservoir-like characteristics with virtually imperceptible velocities. However, it was noted that at points with reduced cross-sections, such as water inlets and outlets, variations in velocities were evident. Specifically, the outlet of Lake Bolonha recorded slightly higher velocities, which aligns with previous studies. On the other hand, the interconnection channel exhibited more significant velocities than did the other channels due to its smaller cross-sectional area. This velocity field served as the basis for simulating the transport of phosphorus originating from the discharge of untreated sewage into the Guamá River within the Água Preta/Bolonha system. A simulation over a one-month period revealed that the pollutant reaches entry into the first treatment plant in approximately one week and then steadily increases until it reaches a peak of 0.02 mg L^{-1} in approximately twenty-five days, after which it remains stable. In contrast, the second treatment plant takes approximately twenty days to be affected by the contaminant, owing to the very low hydrodynamics in Lake Bolonha, requiring an additional five days to reach a maximum concentration of 0.01 mg L^{-1}. It is essential to underscore the consequences of nutrient discharge into lakes, as it contributes to the proliferation of macrophytes and increases water treatment costs. The methodology presented in this study can be applied to simulate other types of pollutants, enabling the analysis of pollutant behaviour in bodies of water and assisting in potential decision-making processes. In this context, a project to increase the volume of treated sewage would be a significant legacy of COP30 for the people of Belém do Pará. Such an initiative would contribute to the reduction of pollutants carried by the waters of the Guamá River and treated in the Utinga Source.

Acknowledgements

The authors would like to thank the Coordination for the Improvement of Higher Education Personnel-Brazil (CAPES) - Finance Code 001. The second author would like to thank the CNPq for funding two research productivity grant (Processes 301049/2025-4 and 300148/2025-9). We would like to thank the office for research (PROPESP) and the Foundation for Research Development (FADESP) of the Federal University of Pará through Grant No. PAPQ 2023.

References

Araújo, T. F., Blanco, C. J. C., Alves, C. S., Holanda, O. S., & Secretan, Y. (2021). Hydrodynamic modeling of the Utinga source in Belém, Pará, Brazil. *Modeling Earth Systems and Environment*, *7*(1), 317–329. https://doi.org/10.1007/s40808-020-01011-5

Elshemy, M., Khadr, M., Atta, Y., & Sayed, A. A. (2016). Hydrodynamic and water quality modeling of Lake Manzala (Egypt) under data scarcity. *Environmental Earth Sciences*, *75*(19), Artigo 1329. https://doi.org/10.1007/s12665-016-6136-x

Heniche, M. A., Secretan, Y., Boudreau, P., & Leclerc, M. (2000). A two-dimensional finite element drying-wetting shallow water model for rivers and estuaries. *Advances in Water Resources*, *23*(4), 359–372. https://doi.org/10.1016/S0309-1708(99)00031-7

Holanda, O. S., Blanco, C. J. C., Mesquita, A. L. A., Brasil Junior, A. C. P., Figueiredo, N. M., Macedo, E. M., & Secretan, Y. (2017). Assessment of hydrokinetic energy resources downstream of hydropower plants. *Renewable Energy*, *101*, 1203–1214. https://doi.org/10.1016/j.renene.2016.10.011

Holanda, P. S., Blanco, C. J. C., Cruz, D. O. A., Lopes, D. F., Barp, A. R. B., & Secretan, Y. (2011). Hydrodynamic modeling and morphological analysis of Lake Água Preta: One of the water sources of Belém-PA-Brazil. *Journal of the Brazilian Society of Mechanical Sciences and Engineering*, *33*(2), 117–124. https://doi.org/10.1590/S1678-58782011000200001

Instituto Trata Brasil. (2024). *Ranking do saneamento do Instituto Trata Brasil de 2024 (SNIS 2022)*. https://tratabrasil.org.br/ranking-do-saneamento-2024/

Lima, N. S., Blanco, C. J. C., Holanda, O. S., Lopes, D. F., Barp, A. R. B., & Secretan, Y. (2013). Hydrodynamic modeling and morphological analysis of Lake Bolonha: A water source in Belém, Pará State, Brazil. *Acta Scientiarum. Technology*, *35*(1), 59–67. https://doi.org/10.4025/actascitechnol.v35i1.13670

Lima, R., Mesquita, A. L. A., Blanco, C. J. C., Lins, E. F., Santos, M. L. S., & Secretan, Y. (2014). On the application of SUPG/q-method in 2D advection-diffusion-reaction simulation. *Journal of the Brazilian Society of Mechanical Sciences and Engineering*, *36*, 591–603. https://doi.org/10.1007/s40430-013-0099-6

Lima, R., Mesquita, A. L. A., Blanco, C. J. C., Santos, M. L. S., & Secretan, Y. (2015). An analysis of total phosphorus dispersion in lake used as a municipal water supply. *Anais da Academia Brasileira de Ciências*, *87*(3), 1505–1518. https://doi.org/10.1590/0001-3765201520130317

Massabó, M., Cianci, R., & Paladino, O. (2011). An analytical solution of the advection dispersion equation in a bounded domain and its application to laboratory experiments. *Journal of Applied Mathematics*, *2011*, Artigo 493014. https://doi.org/10.1155/2011/493014

McCartin, B. J., & Forrester Jr, S. B. A. (2002). Fractional step-exponentially fitted hopscotch scheme for the Streeter-Phelps equations of river self-purification. *Engineering Computations*, *19*(2), 177–189. https://doi.org/10.1108/02644400210419049

Organização das Nações Unidas. (2015). *Transformando nosso mundo: A Agenda 2030 para o Desenvolvimento Sustentável*. https://brasil.un.org/pt-br/91863-agenda-2030-para-o-desenvolvimento-sustentavel

Roohi, M., Soleymani, K., Salimi, M., & Heidari, M. (2020). Numerical evaluation of the general flow hydraulics and estimation of the river plain by solving the Saint–Venant equation. *Modeling Earth Systems and Environment*, *6*(2), 645–658. https://doi.org/10.1007/s40808-020-00718-9

Saad, Y., & Schultz, M. H. (1986). GMRES: A generalized minimal residual algorithm for solving nonsymmetric linear systems. *SIAM Journal on Scientific and Statistical Computing*, *7*(3), 856–869. https://doi.org/10.1137/0907058

Santos, M. L. S., Sousa, R. R., Pereira, J. A. R., Silva, J. P., & Lima, M. W. (2015). Diffuse sources of pollution and their influence on the nature of the sediments in Água Preta Lake. *Acta Scientiarum. Technology*, *37*(2), 259–264. https://doi.org/10.4025/actascitechnol.v37i2.25745

Secretan, Y. (2023). *H2D2 Software* [Software]. GitLab. https://www.gitlab.com/h2d2

Tarabih, O. M., Dang, T. C., Paudel, R., & Arias, M. E. (2023). Lake operation optimization of nutrient exports: Application of phosphorus control in the largest subtropical lake in the United States. *Environmental Modelling & Software*, *160*, Artigo 105603. https://doi.org/10.1016/j.envsoft.2022.105603

Tezduyar, T. E. (1992). Stabilized finite element formulations for incompressible flow computations. *Advances in Applied Mechanics*, *28*, 1–44. https://doi.org/10.1016/S0065-2156(08)70153-4

Yi, Y., Tang, C., Yang, Z., Zhang, S., & Zhang, C. (2017). A one-dimensional hydrodynamic and water quality model for a water transfer project with multihydraulic structures. *Mathematical Problems in Engineering*, *2017*, Artigo 656191. https://doi.org/10.1155/2017/2656191